Arch. Metall. Mater. **65** (2020), 4, 1329-1333

DOI: 10.24425/amm.2020.133694

ASHUTOSH SHARMA[1], BYUNGMIN AHN[1*]

A FACILE METHOD FOR THE PRODUCTION OF Sn-Ag ALLOY BY HIGH ENERGY BALL MILLING

In this study, we have developed Sn-Ag alloy by a simple high energy ball milling technique. We have ball-milled the eutectic mixture of Sn and Ag powders for a period of 45 h. The milled powder for 45 h was characterized for particle size and morphology. Microstructural investigations were carried out by scanning electron microscopy and X-ray diffraction studies. The melting behavior of 45 h milled powder was studied by differential scanning calorimetry. The resultant crystallite size of the Sn(Ag) solid solution was found to be 85 nm. The melting point of the powder was 213.6ºC after 45 h of milling showing depression of ≈6ºC in melting point as compared to the existing Sn-3.5Ag alloys. It was also reported that the wettability of the Sn-3.5Ag powder was significantly improved with an increase in milling time up to 45 h due to the nanocrystalline structure of the milled powder.

Keywords: Pb-free, solder, electronics, ball milling, microstructure

1. Introduction

Recent RoHS and WEEE regulations of Pb in electronic devices coupled with the environmental concerns direct the electronic manufacturers to produce Pb-free solders for electronic devices [1-2]. The most popular Pb-free alloy with regard to excellent mechanical strength and wetting is Sn-Ag-Cu alloy. However, the Sn-Ag-Cu alloy has dual intermetallic compounds, i.e., Cu_6Sn_5 (IMC) apart from Ag_3Sn. Therefore, the solder joint reliability becomes a bit more complex [3]. Another category of Pb-free alloys includes Sn-Cu and Sn-Ag alloys. However, the melting point of Sn-0.7Cu is higher than Sn-3.5Ag alloy. Other common alloys include Sn-Zn, Sn-Bi, and Sn-In which are oxidation prone, brittle or extremely expensive due to the limited supply of raw materials [7]. Therefore, among the various kinds of Pb-free alloys, Sn-Ag alloy seems to be a potential candidate for Pb-free applications [4-6]. The presence of Ag has been shown to improve the wetting of the alloy on the common metallic conductors, e.g., Cu, Ni, Au, etc.

Sn-Ag alloys are currently used as a joining material in interconnections and electronic packaging devices [4-6]. Therefore, the performance of Sn-Ag solder depends mainly on the characteristics of Sn-Ag powders. There are various methods of fabrication of Sn-Ag alloys in literature, such as powder metallurgy, sol-gel, melting and casting, plating, high energy ball milling (HEBM), vapor deposition/plasma, and atomization techniques [7-8]. Commercial Sn-Ag powders are mostly produced by atomization and plasma-based methods which form submicron to nanosize powders. However, most of these methods have issues of segregation during reflow procedures due to the different densities of Sn and Ag powder [9-11]. Among other methods, HEBM is one of the simplest and convenient methods for the fabrication of alloys. HEBM minimizes powder segregation and is an excellent technique for mass-scale production [12,17]. The reduction in the melting point of alloy powders achieved via HEBM can be violated to produce novel, nanocrystalline, low melting Pb-free solders as compared to their bulk counterparts [12]. In the past, HEBM has been attempted successfully to produce Sn-based alloy powders [13-15].

Lai and his co-worker Duh have synthesized Sn-3.5Ag solder paste by HEBM and investigated the melting and wetting properties [16]. Various research activities have been attempted in the past on the powder metallurgy and a few related to HEBM of Sn-Ag alloy reinforced with ceramic nanoparticles (Al_2O_3, ZrO_2, SiC, TiO_2, SWCNT, MWCNT, etc.) [17]. A considerable depression in the melting point and improvement of wetting properties have been documented. In addition, the dispersion of ceramics into a soft metal matrix has several unresolved issues.

[1] AJOU UNIVERSITY, DEPARTMENT OF MATERIALS SCIENCE AND ENGINEERING AND DEPARTMENT OF ENERGY SYSTEMS RESEARCH, 206 WORLDCUP-RO, YEONGTONG-GU, SUWON, GYEONGGI, 16499, KOREA

* Corresponding author: byungmin@ajou.ac.kr

Ceramic nanoparticles have been shown to segregate during the solder reflow and low-temperature microjoining [18-19]. In addition, limited information exists on the improvement of the solderability of Sn-Ag alloy produced via HEBM of the Sn-Ag powder. Therefore, some important points related to HEBM of Sn-Ag alloys, e.g., microstructure evolutions, depression in melting point and spreading behavior of Sn-Ag alloy to copper substrates need to be clarified in detail.

Thus, in this paper, we have developed the Sn-Ag alloy using the HEBM approach. The milled powders are sought to have lower liquidus temperature and high strength when applied to the solder joints. The melting point and microstructure evolution study of the milled powders were be carried out using the various advanced characterization techniques.

2. Experimental

In this work, the powder constituents were milled in the composition of Sn-3.5wt%Ag for 45 h. HEBM was performed at 300 rpm and 10:1 ball to powder mass ratio. The milling media consists of 50 WC balls and vials and the milling was done with 0.2wt% stearic acid as a process control agent. Table 1 shows the composition of the selected alloy in this study.

TABLE 1

Selected composition of the Sn-Ag alloy powder

Element	Composition (wt.%)	
	Ag	Sn
Values	3.5	96.5

After milling, the powder was characterized for their crystallite size and lattice strain using the Scherer equation. A benchtop X-ray diffractometer (XRD) (Miniflex, Rigaku, Japan) was used for phase evolution studies. For XRD analysis, the sample powder was packed over the glass slit holder (10 mm × 10 mm × 2 mm). The powder sample was handled with great care so as not to contaminate with the external environment. The XRD tests were carried out using Cu Kα radiation (λ = 1.54056 Å) at an applied voltage and current of 40 kV and 35 mA, respectively. The powder samples were X-ray scanned from 25 to 70° of the Bragg angle.

The powder morphology was observed in scanning electron microscope (SEM) (Hitachi S-4800, Japan). Prior to microscopy, the samples were stored in the glove box to avoid any environmental contamination during the XRD experiment. The composition of powder was estimated by the (EDX) energy-dispersive X-ray spectroscopy (INCA, Oxford).

Further, the melting point of the Sn-Ag specimen was assessed by differential scanning calorimetry (DSC) (Perkin Elmer, Germany) at a scanning rate of 10°C/min and from 50°C to 500°C in Argon atmosphere using alumina pans. The milled powder was also reflowed and the spread ratio of the powder was noted to assess the wetting property on a copper substrate.

3. Results and discussion

The XRD patterns of Sn-Ag alloy after milling for 45 h are presented in Fig. 1. The pattern indicates broad tetragonal β-Sn peaks along with a few Ag_3Sn IMCs. The various peaks are associated with β-Sn(Ag) solid solutions. The average crystallite size of 45 h ball-milled powder was around 85 nm as calculated from the Williamson Hall equation as follows [20]:

$$\beta(hkl)\cos\theta = K\lambda/D + 4\varepsilon\sin\theta \quad (1)$$

Here, K = 0.9 assuming Cauchy – like profile, λ = 1.5406 Å, θ = Bragg angle, D = mean crystallite size, ε = lattice strain. The instrument corrected broadening is given by $\beta^2(hkl) = \beta^2_{\text{measured}} - \beta^2_{\text{instrument}}$, where β = full width at half maximum.

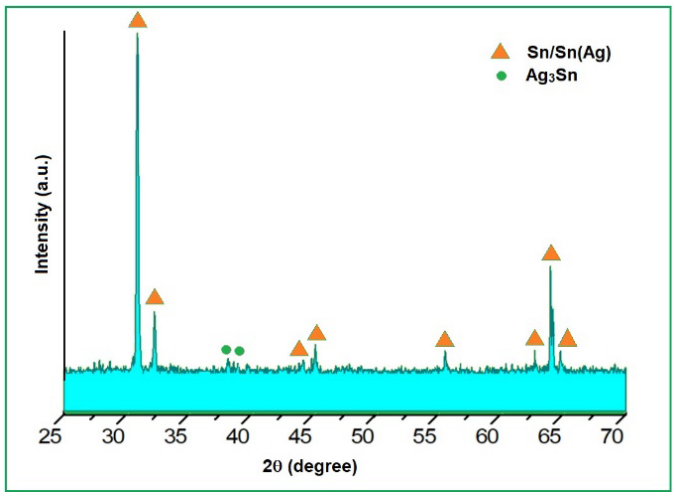

Fig. 1. XRD pattern of Sn-Ag alloy milled for 45 h

The various crystallite size and lattice strains are shown in Table 2. The lattice constants of the milled powder were determined by Nelson Riley's method. It was seen that there was no significant variation in the lattice parameter (a and c). A similar result was noticed in the past by Reddy et al. while working on the HEBM of Sn-Ag-Cu alloys [21].

TABLE 2

Crystallite size, lattice strain, and lattice parameter

Milling time (h)	Crystallite size (nm)	Lattice strain (%)	Lattice parameter (nm)	
5	176	0.0015	a = 0.58310	c = 0.31816
15	165	0.0039	0.58312	0.31813
25	152	0.0076	0.58310	0.31811
35	135	0.0148	0.58309	0.31810
45	85	0.0163	0.58308	0.31808

The crystallite size of the β-Sn(Ag) solid solution decreases at a slower rate during the initial stages of HEBM up to 25 h and at a faster rate at higher milling times up to 45 h. The lattice strains were also found to increase with milling time. The continuous welding and fracturing during HEBM generate

tremendous lattice strains and defects followed by a balance of cold welding and fracturing at higher milling times is crucial for the nanostructural properties of the powder [12].

The alloying behavior of Sn-Ag powder is associated with the formation of (1) β-Sn(Ag) solid solution and (2) Ag_3Sn IMCs. The solid solubility of Ag in Sn is almost negligible even at the eutectic point [22]. However, the non-equilibrium HEBM processing induces lattice defects in the nanostructured powder particles leading to the formation of β-Sn(Ag) solid solution and simultaneous precipitation of Ag_3Sn. In addition, noble atoms (group IB, e.g. Ag, Cu, and Au) can diffuse easily to group IIIA elements (e.g., Sn, In and Pb) through an interstitial diffusion and form the IMCs [23].

The surface morphology of the Sn-3.5Ag powder was observed in SEM machine as shown in Fig. 2. It was shown that the crystal size decreased with prolonged milling times. However, until 35 h, some cold welding was also shown but with continued milling, the particles got work-hardened and fractured to fine particles. The EDX analysis confirms the presence of the β-Sn and Ag_3Sn phase without any contamination. The EDX analysis of Fig. 2e-f is presented in Table 3.

TABLE 3

Compositional analysis of Sn-Ag milled powder

Phase	Composition (wt.%)	
	Sn	Ag
1	96.7	3.3
2	100	0
3	79	21

The melting behavior of the Sn-3.5wt%Ag alloy is shown by the DSC curve of milled Sn-Ag after 45 h (Fig. 3). It is shown that the melting point is decreased significantly after milling for 45 h. The eutectic melting point of the standard Sn-3.5wt% Ag is around 221°C [1]. Therefore, our results show a depression of melting point around 6°C at Ag ≈ 3.5%. The melting point of a metal is the characteristic property that depends upon the interatomic distance and the amplitude of root mean vibration of atoms. In addition to the particle size refinement, the formation of secondary Ag_3Sn in the matrix, therefore, alters the interatomic distance. These combined effects give rise to a decrease in melting temperature after the addition of Ag. However, too much formation of Ag_3Sn is not desirable as it can severely raise the melting point. At a concentration of Ag > 3.5wt.%, Ag_3Sn grows to a plate shape rather than fine particles and hence melting point depression will not be sufficient [24].

The nanostructuring of the powder particles lowers the Gibbs free energy and hence melting point is depressed. This fact is supported by the decrease in the crystallite size of the powders. The lattice microstrain and enthalpy of melting vary with grain size inversely. In other words, the stored enthalpy rises with prolonged HEBM [21].

The spread ratio of the powders was also evaluated after reflowing at 250°C on copper substrates. The reflow profile used for the spread test is shown in Fig. 4. The spreading ratio results are shown in Fig. 5 as calculated by the relation [25-26]:

$$\text{Spread ratio (\%)} = (A_f - A_i)/A_i \quad (2)$$

Here, A_f is the area after spread and A_i is the initial area. The reflowed images of Sn-Ag alloy are shown in Fig. 5a. It can be

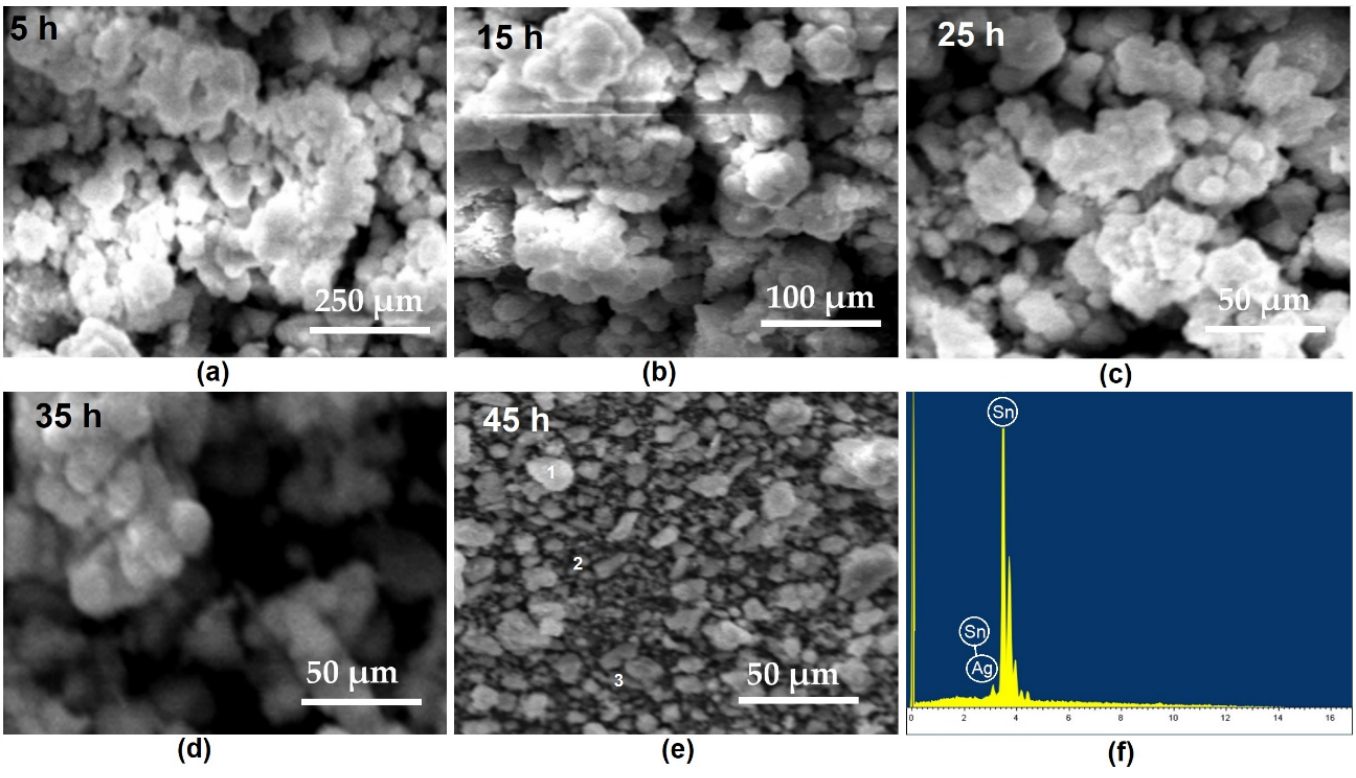

Fig. 2. SEM micrograph of Sn-Ag alloy milled for various times and EDX analysis

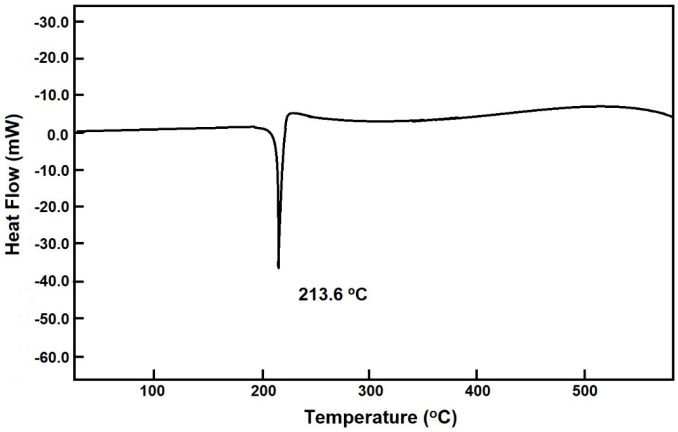

Fig. 3. The DSC curve of the HEBMed Sn-Ag alloy powder after 45 h

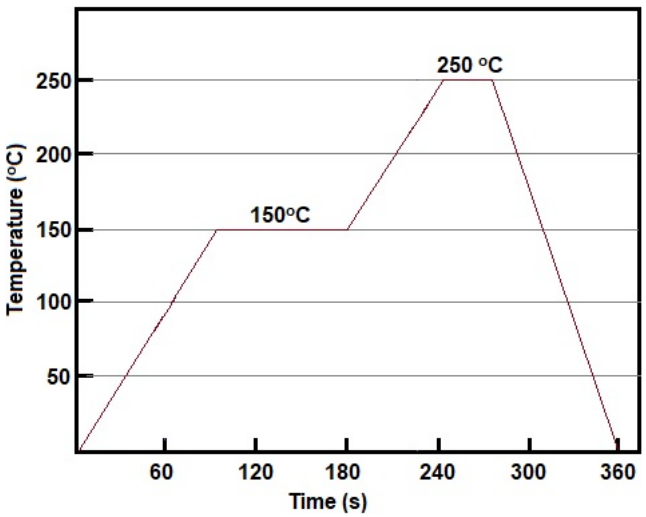

Fig. 4. The reflow profile for the measurement of the spreadability of the Sn-3.5wt% alloy

observed that the solder spread areas improve with the milling time. The spread ratio is very low for the samples ball milled for 5-15 h and increases continuously up to the final spread ratio ~95% for 45 h milled powder (Fig. 5b). This observation suggests that higher surface energy of the nanocrystalline powder causes a depression in the surface tension between the copper and the alloy powder that results in the increased wetting of the alloy powder [4-5].

Spreading of liquid metal on the solid surface indicates the ability to wet and make close contact with the solid substrate. Thomas Young established the relation between the various intermolecular forces acting among the various interfaces (solid, liquid and vapor). According to the wetting equation [27]:

$$\gamma_{sv} - \gamma_{sl} = \gamma_{lv} \cos\theta \tag{6}$$

where, γ_{sv}, γ_{lv}, and γ_{lv} represent the interfacial energy of the solid-vapor, liquid-vapor, and solid-liquid interface. The angle θ corresponds to the wetting angle. Alternatively, from equation (6), if wetting angle decreases, spreading increases. Therefore, the nanostructuring of powder with an increase of milling time causes the formation of high surface energy nanoparticles. These high surface-active nanoparticles decrease the (1) interface energy at the liquid-solid interface and (2) wetting angle and hence more spreading. Therefore, we observe an improved spreading with prolonged milling times.

It is a noteworthy point to mention that the wetting of the solder on conducting surface is a prime factor for soldering applications. In modern electronic devices, a good wetting ensures complete bonding of the Sn-Ag alloy to the copper conductors. However, too much formation of Ag_3Sn IMC will lead to a decrease in wetting property. Therefore, we restricted the Ag content to eutectic composition. These results indicate that HEBM is a beneficial tool for enhancing the microstructural, thermal and wetting characteristics of the Sn-Ag alloy for possible Pb-free applications.

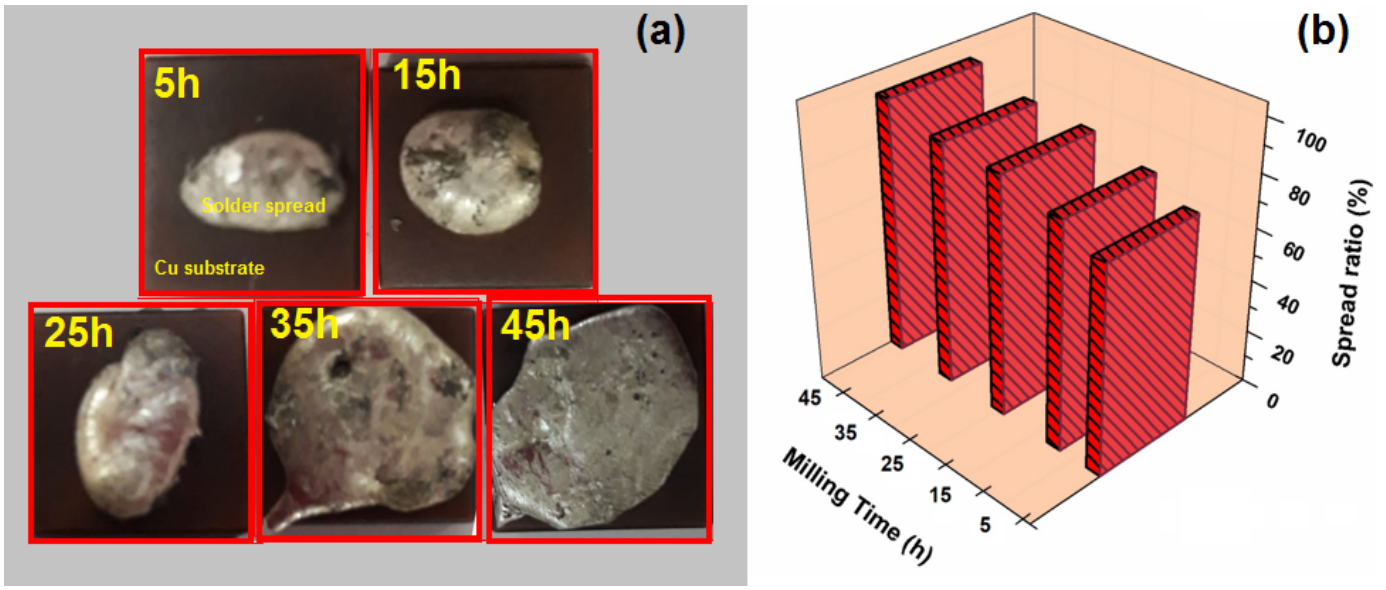

Fig. 5. The spreadability of the Sn-3.5wt%Ag powder after various milling times. (a) Spreading images and (b) calculated spread ratio

4. Conclusions

In this work, we have produced Sn-3.5wt%Ag alloys by employing a high energy ball milling approach. The morphology of Sn-3.5wt%Ag powders revealed the presence of secondary Ag_3Sn IMCs distributed with the major β-Sn phase. The size of the Sn-3.5Ag powder was considerably refined up to 45 h of milling down to 85 nm by HEBM method without any presence of additional impurity from the balls or WC containers. The XRD analysis confirmed the crystallite size of 45 nm and an increased strain due to the deformation of the lattice. The nanostructuring of powder was also associated with depression in melting point by 6ºC after 45 h milling. The spread ratio of the powder was also improved significantly up to 95% due to the effect of HEBM route. It can be concluded that the HEBM approach can significantly improve the soldering properties for possible microelectronic Pb-free applications.

Acknowledgments

This research was supported by Basic Science Research Program through the National Research Foundation of Korea (NRF) funded by the Ministry of Education (NRF-2018R1D1A1B07044481) (B.A.). This research was supported by Basic Science Research Program through the National Research Foundation of Korea (NRF) funded by the Ministry of Education (NRF-2018R1D1A1B07044706) (A.S.).

REFERENCES

[1] M. Abtew, G. Selvaduray, Mater. Sci. Eng. R **27**, 95-141 (2000).
[2] K. Zeng, K.N. Tu, Mater. Sci. Eng. R **38**, 55-105 (2002).
[3] A. Sharma, S. Mallik, N.N. Ekere, J.P. Jung, J. Microelectron. Packag. Soc. **21** (4), 83-89 (2014).
[4] A. Sharma, A.K. Srivastava, B. Ahn, Metall. Mater. Trans. A **50** (11), 5384-5394 (2019).
[5] A. Sharma, H. Yu, I.S. Cho, H. Seo, B. Ahn, Electron. Mater. Lett. **15** (1), 27-35 (2018).
[6] A. Sharma, S. Bhattacharya, S. Das, K. Das, Metall. Mater. Trans. A **44**, (12) 5587-5601 (2013).
[7] A. Sharma, S. Das, K. Das, in: A. M. A. Mohamed (Ed.), Electrodeposition of Composite Materials, InTech 253-274, Croatia (2016). DOI: 10.5772/62036
[8] A. Sharma, S. Das, K. Das, Pulse electroplating of ultrafine grained tin coating, in: M. Aliofkhazraei (Ed.), Electroplating of Nanostructures, InTech, Croatia (2015). DOI: 10.5772/61255
[9] P. Fauchais, G. Montavon, M. Vardelle, J. Cedelle, Surf. Coat. Technol. **201**, 1908-1921 (2006).
[10] J. Karthikeyan, C.C. Berndt, J. Tikkanen, S. Reddy, H. Herman, Mater. Sci. Eng. A **238**, 275-286 (1997).
[11] S. Lagutkin, L. Achelis, S. Sheikhaliev, V. Uhlenwinkel, V. Srivastava, Mater. Sci. Eng. A **383**, 1-6 (2004).
[12] C. Suryanarayana, Prog. Mater. Sci. **46**, (1-2) 1-184 (2001).
[13] M.L. Huang, C.M.L. Wu, J.K.L. Lai, J. Mater. Sci. **11**, 57-65 (2000).
[14] S.T. Kao, J.G. Duh., J. Electron. Mater. **33**, 1445-1451 (2004).
[15] C.M.L. Wu, M.L. Huang, J.K.L. Lai, Y.C. Chan, J. Electron. Mater. **29**, 1015-1020 (2000).
[16] H.L. Lai, J.G. Duh, J. Electron. Mater. **32**, 215-220 (2003).
[17] J. Shen, Y.C. Chan, Microelectron. Reliab. **49**, 223-234 (2009).
[18] A. Sharma, M.H. Roh., D.H. Jung, J.P. Jung, Metall. Mater. Trans. A **47A**, 510-521 (2016).
[19] A. Sharma, D.. Lim, J.P. Jung, Mater. Sci. Technol. **32**, 773-779 (2016).
[20] V.D. Mote, Y. Purushuttom, B.N. Dole, J. Theor. Appl. Phys. **6**, 1-8 (2012).
[21] B. Reddy, P. Bhattacharya, B. Singh, K. Chattopadhyay, J. Mater. Sci. **44**, 2257-2263 (2009).
[22] W.F. Gale, T.C. Totemeier, Smithells Metal Reference Book, 8th ed., Elsevier Butterworth-Heinemann, Burlington, MA, USA (2004).
[23] T. Laurila, V. Vuorinen, J.K. Kivilahti, Mater. Sci. Eng. R **49**, 1-60 (2005).
[24] K. Suganuma, S.-H. Huh, K. Kim, H. Nakase, Y. Nakamura, Mater. Trans. **42**, 286-291 (2001).
[25] A. Sharma, A.K. Srivastava, K. Lee, B. Ahn, Met. Mater. Int. **25** (4), 1027-1038 (2019).
[26] A. Sharma, A.K. Srivastava, B. Ahn, Mater. Res. Exp. **6**, 056520 (2019).
[27] S. Mishra, A. Sharma, D.H. Jung, J.P. Jung, Met. Mater. Int. (2019), DOI: 10.1007/s12540-019-00536-4 (in press).